Original Article

β3 adrenoceptor agonist mirabegron protects against right ventricular remodeling and drives Drp1 inhibition

Lin Zhao[1#]^, Hui Luo[2#], Tangzhiming Li[3]^, Xiexiong Zhao[1], Yanghong Liu[4]

[1]Department of Cardiovascular Medicine, the Third Xiangya Hospital, Central South University, Changsha, China; [2]Department of Cardiology, the First Hospital of Changsha, Changsha, China; [3]Department of Cardiology, the Second Clinical Medical College (Shenzhen People's Hospital), Jinan University, Shenzhen, China; [4]Center for Reproductive Medicine, the Third Xiangya Hospital, Central South University, Changsha, China

Contributions: (I) Conception and design: L Zhao; (II) Administrative support: L Zhao, H Luo; (III) Provision of study materials or patients: H Luo; (IV) Collection and assembly of data: T Li, X Zhao; (V) Data analysis and interpretation: L Zhao, X Zhao, Y Liu; (VI) Manuscript writing: All authors; (VII) Final approval of manuscript: All authors.

[#]These authors contributed equally to this work.

Correspondence to: Lin Zhao. Department of Cardiovascular Medicine, the Third Xiangya Hospital, Central South University, Changsha 410013, China. Email: l.zhao17@alumni.imperial.ac.uk.

Background: The right ventricular (RV) function determines the prognosis of patients with pulmonary hypertension (PH). Metabolic disorders have been observed in the RV myocardium in PH. Activation of the β3 adrenoceptor improves cardiac function and restores cardiac metabolic efficiency in rodents with heart failure; however, its role in the RV remains uncertain.

Methods: Experimental PH was induced by monocrotaline (MCT) in rats. Mirabegron, a selective β3 adrenoceptor agonist, was given to MCT rats daily from the day after MCT injection at the dose of 10 mg/kg. *In vivo* echocardiography and RV catheterization were performed to assess RV hemodynamics, structure, and function. RV fibrosis and hypertrophy were assessed by Sirius Red (SR) and wheat germ agglutinin (WGA) staining respectively. Western blotting was performed to examine the markers of RV fibrosis and hypertrophy, as well as the levels of the key molecules and their phosphorylated forms. The molecular changes were confirmed in the cardiac hypertrophy model of angiotensin II (Ang II) treated H9c2 cardiomyocytes using western blotting.

Results: The overloaded RV had increased β3 adrenoceptor expression, which was further increased by mirabegron. Mirabegron reduced RV pressure and reduced RV structural and functional deterioration in MCT rats. Mirabegron decreased cardiac fibrosis and hypertrophy in the overloaded RV. Mirabegron suppressed dynaminrelated protein 1 (Drp1) and promoted AMP-activated protein kinase (AMPK) signaling in the overloaded RV and Ang II treated cardiomyocytes.

Conclusions: The β3 adrenoceptor agonist mirabegron reduced RV hypertrophy and fibrosis in PH rats. The treatment effect involved Drp1 inhibition and AMPK activation.

Keywords: Mirabegron; right ventricle; pulmonary hypertension (PH); dynaminrelated protein 1 (Drp1); AMP-activated protein kinase (AMPK)

Submitted Jun 04, 2022. Accepted for publication Oct 21, 2022.
doi: 10.21037/cdt-22-274
View this article at: https://dx.doi.org/10.21037/cdt-22-274

^ ORCID: Lin Zhao, 0000-0003-2994-2387; Tangzhiming Li, 0000-0002-5273-9531.

Introduction

Pulmonary hypertension (PH) is a fatal disease characterized by a progressive increase in pulmonary vascular resistance and pulmonary arterial pressure (1). The right ventricle (RV) function is the most important indicator of prognosis in PH patients. Current PH medicines do not specifically target RV pathology (2,3). RV-specific therapeutic solutions for PH are urgently needed.

Mitochondrial dysfunction is one of the intricate factors involved in the pathogenesis of RV in PH (2). Mitochondria remain in a state of constant fusion and fission, referred to as mitochondrial dynamic. This dynamic is well-aligned with mitochondrial functionality and integrity (4). Dynamin-related protein 1 (Drp1) is essential for mitochondrial fission. The regulation of this important protein is tightly linked to cellular processes such as mitophagy, oxidative stress, and calcium overloading.

Excessive activation of Drp1 has been observed in the pathophysiology of PH. Drp1 promotes proliferation and apoptosis resistance in pulmonary artery smooth muscle cells (5). There is evidence that Drp1 could be suppressed by AMP-activated protein kinase (AMPK) activation, leading to reduced reactive oxygen species (ROS)-induced mitochondrial fission in the endothelium (6). In RV fibroblasts, increased Drp1-mediated mitochondrial fission was detected. Drp1 inhibition reduces mitochondrial fission, which prevents RV fibrosis and collagen synthesis (7). Drp1 inhibition may enhance RV metabolism and improve RV function in patients with PH, making it an attractive therapeutic target.

β3 adrenoceptor (B3AR) plays a cardioprotective role in the dysfunctional heart and serves as a potential therapeutic target (8). Depletion of B3AR induces cardiac dysfunction through regulation of energy metabolism (9). Upregulation of B3ARs reduces neurohormone-induced cardiac hypertrophy (10). Mirabegron is an approved high-selective agonist of B3AR with studies supporting its cardiovascular benefits (11). Mirabegron reduced pulmonary vascular resistance and improved RV ejection fraction in a porcine model of experimental PH induced by pulmonary vein banding (12). Further effort is warranted to validate the effect of mirabegron on the metabolic and functional dysfunction in the overloaded RV in the PH condition.

Here, we present a study investigating the therapeutic potential of mirabegron in the failing RV in experimental PH. This study aimed to explore the impact of mirabegron on dysfunctional RV. The study postulated the interaction between mirabegron and key molecules in metabolic regulation. The results were supportive of the beneficial effect of mirabegron on the failing RV in PH, proposing mirabegron as a potential medication for PH. We present the following article in accordance with the ARRIVE reporting checklist (available at https://cdt.amegroups.com/article/view/10.21037/cdt-22-274/rc).

Methods

Monocrotaline (MCT)-induced PH in rats and mirabegron treatment

Experiments were performed under a project license (No. CSU-2022-01-0122) granted by the Animal Ethics Committee of Central South University, in accordance with the Animals (Scientific Procedures) Act 1986 for the care and use of animals. Sample size calculation and power estimation were performed beforehand using the OpenEpi platform (http://openepi.com/). According to our experience, the standard deviation (SD) of the mean pulmonary artery pressure (mPAP) was around 8 mmHg. The mPAP was assumed normally distributed. The significant level (α) and the statistic power (β) were set as 0.05 and 0.80 respectively. It was concluded that the sample size (N) of 5 per group was able to detect a difference that was no less than 15 mmHg. Therefore, at least 5 animals were assigned to each group. A total number of 48 healthy adult male Sprague-Dawley rats weighing 150–200 grams were used for the experiments in this study. The sample size in each group is stated in figure legends. The rats were housed in the 12/12 h light/dark cycle with food and water freely available. After a 1-week acclimatization period, we use the random numbers method to randomly allocate the rats into three groups: (I) healthy control group (HC); (II) disease model of MCT-induced PH rats (MCT); (III) disease model of MCT rats with mirabegron treatment (MCT + Mira). For the establishment of the PH rat model, the rats in indicated groups received a single subcutaneous injection of MCT (Sigma-Aldrich) at a dose of 60 mg/kg. Mirabegron was diffused in a small volume of drinking water and was given to MCT rats by oral gavage. The gavage started on the day after the MCT injection, at the dose of 10 mg/kg, daily. The gavage lasted on the day that the rats received RV catheterization. The dosage of mirabegron on rats was chosen according to both the dose conversion from the highest human dose (13,14), and the literature reports (15,16). The grouping information of the rats was blinded to the researcher who analyzed the data.

Real-time quantitative polymerase chain reaction (RT-qPCR)

Total RNA was isolated from rat RV tissues using TRIzol reagent (Takara, Shiga, Japan) according to the manufacturer's protocol. The quality of the isolated RNA was assessed using NanoDrop2000 (Thermo Fisher Scientific, Massachusetts, USA) by measuring the absorbance at 260 nm (A260), 280 nm (A280), and 230 nm (A230). Reverse transcription was performed with the isolated RNA to produce the first strand complementary DNA (cDNA) using RevertAid First Strand cDNA Synthesis Kit (Thermo Fisher Scientific). Real-time PCR was performed on the cDNA template using SYBR Premix Ex Taq Kit (Takara) with the Applied Biosystems 7300 Real-Time PCR System (Applied Biosystems). The primer pairs sequences of B3AR and GAPDH are listed in Table S1. Each sample was analyzed in triplicate. The relative expression of the target transcripts was calculated using the comparative Ct method with normalization to GAPDH transcripts.

Assessment of hemodynamics and RV hypertrophy

RV catheterization was performed to evaluate RV hemodynamics in MCT rats. The rats were anesthetized intraperitoneally with 50 mg/kg pentobarbital. Appropriate anesthetic depth was confirmed by assessing the loss of the pedal reflex. A pre-curved heparin-rinsed catheter was inserted into the right jugular vein of the rats. After insertion, the catheter was pushed sequentially through the right atrium, the RV, and the pulmonary artery (PA). The pressure information was continuously captured (PowerLab, ADInstruments, Sydney, Australia). The mPAP was calculated automatically by the software, which is defined as the arithmetic mean pressure of all the points in the pre-selected PA pressure curves. Systemic systolic blood pressure (SBP) was obtained by inserting a catheter into the carotid artery of the rats. The hemodynamic records were analyzed using PowerLab Pro (v8.1.19 ADInstruments).

Echocardiographic measurements

RV-specific echocardiography was performed in a blinded manner by an experienced researcher. Rats were anesthetized with 50 mg/kg pentobarbital intraperitoneally. Transthoracic echocardiography (Vevo 2100, VisualSonics Inc.) was performed. Images of the apical 4-chamber view, parasternal left ventricle long-axis view, and parasternal aortic valve short-axis view were acquired. RV end-diastolic area (RVEDA) and RV end-systolic area (RVESA) were measured in the apical 4-chamber view. The RV fractional area change (RVFAC) was calculated from RVEDA and RVESA. Stroke volume (SV) was estimated from the left ventricle in M-mode parasternal long axis view. Body surface area (BSA) was calculated using Meeh's formula ($BSA = 10 \times weight^{2/3}$). Cardiac index (CI) was calculated as: SV × heart rate/BSA. The velocity of the PA was measured using pulse-wave Doppler in the parasternal aortic valve short-axis view. Pulmonary artery acceleration time (PAAT) was measured from PA velocity as the time of the velocity change from the base to the peak.

Immunohistochemistry and immunofluorescence

The RV was fixed in 10% formaldehyde and was subsequently embedded in paraffin. The paraffin block was then trimmed and sectioned at a thickness of 5 µm. The sections were stained with Sirius Red (SR) to identify collagen fibers. The sections were stained with fluorescein isothiocyanate (FITC)-labeled wheat germ agglutinin (WGA) to visualize the cardiomyocytes. The stained sections were photographed in a blinded manner. Ten random fields from the RV free wall were acquired for each rat at 20× magnification for analysis. The arithmetic mean of the ten fields was calculated as the quantitation of the rat. The histology images were processed and analyzed using FIJI (ImageJ).

Immunoblotting

Immunoblotting was performed on the protein extractions of the RV tissue and the H9c2 cells. The RV tissue or the cell pellet was homogenized in RIPA buffer supplemented with phosphorylase and protease inhibitors (CWBIO, Beijing, China) on ice for 20 minutes. The homogenate was centrifuged at 14,000 ×g for 15 minutes. The supernatant was quantified immediately after extraction using the Bicinchoninic Acid protein assay (Thermo Fisher Scientific). For electrophoresis, 20 µg protein was loaded onto a sodium dodecyl sulfate-polyacrylamide gel (SDS-PAGE). The separated proteins were transferred onto polyvinylidene fluoride (PVDF) membranes (Millipore) and sequentially incubated with the relevant antibodies as indicated. The primary antibodies used in this study are listed in Table S2. Protein expression was analyzed using FIJI (ImageJ).

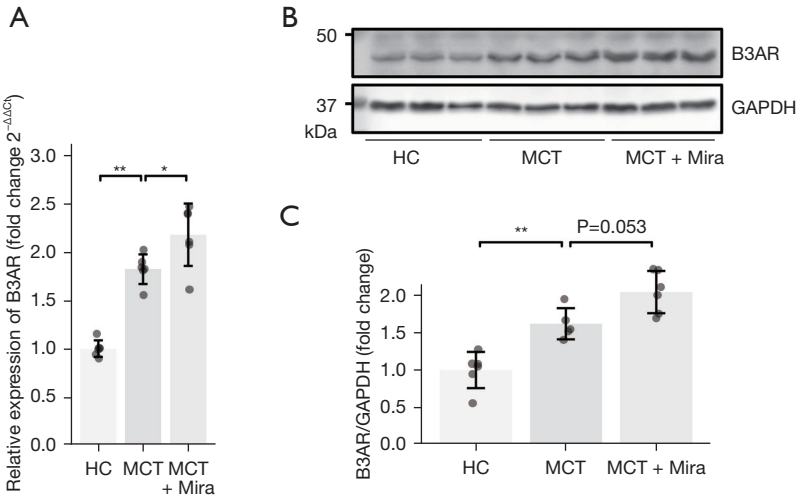

Figure 1 The increased expression of B3AR in the RV in MCT rats was further elevated by mirabegron. (A) Detection of the RNA expression of β3AR using RT-qPCR. (B) Representative immunoblots of β3AR in the three groups. (C) Quantification of the density of the immunoblots in the three groups. MCT: MCT rats; MCT + Mira: MCT rats with mirabegron treatment. Sample size: N=6 for each group. Significance codes: *, P<0.05; **, P<0.01. β3AR, β3 adrenoceptor; HC, healthy control; MCT, monocrotaline; RV, right ventricular.

Cardiomyocyte hypertrophy model of H9c2 cells

H9c2 cells (rat cardiomyocytes) were obtained from the Cell Bank of China Science Academy (Shanghai, China). H9c2 cells were cultured in Dulbecco's modified eagle's medium (DMEM) with 10% fetal bovine serum (FBS). H9c2 cells with 60–70% confluency were serum starved and were then treated with angiotensin II (Ang II) (600 nM), mirabegron (10 μM), Compound C (10 μM), and/or mdvid1 (20 μM) simultaneously as stated in the figures for 24 hours. The doses of the treatments were based on published studies (17-20). The cells were harvested for immunoblotting.

Statistical analysis

Statistical analyses were performed using *R 4.1.1*. All values are presented as mean (SD) unless otherwise stated. Shapiro-Wilk's test was performed to check the normality of the data in each group before *t*-tests or one-way analysis of variance (ANOVA). The normal distribution of the data in the groups was confirmed, and parametric one-way ANOVA was used for multi-group analysis. Tukey's Honest Significant Difference method was used for multiple comparisons. Significant differences were observed at P<0.01. Significance code in the figures: *, P<0.05; **, P<0.01; ***, P<0.001.

Results

The failing RV presented increased B3AR expression

To assess the role of the B3AR and its agonist in the pathogenesis of RV hypertrophy, the expression of B3AR in the RV of MCT rats was examined by RT-qPCR and immunoblotting. The RT-qPCR detected an increased RNA expression of B3AR in MCT rats. MCT rats with mirabegron treatment had an even higher expression of B3AR than MCT rats without mirabegron treatment (*Figure 1A*). The representative immunoblots were presented in *Figure 1B*. Compared to the healthy controls, an increased protein level of B3AR was observed within the RV homogenate of MCT rats (*Figure 1C*). Similar to the RT-qPCR results, immunoblotting detected a further elevation of B3AR in MCT rats with mirabegron treatment (P=0.053).

Mirabegron attenuated RV hemodynamic disturbances and RV structural deterioration in MCT-induced PH

Mirabegron (10 mg/kg/day) was administered to the rats by gavage on the first day of MCT injection. Three weeks later, RV and PA hemodynamic parameters were obtained through RV catheterization. *Figure 2A* respectively shows the representative pressure curves of RV and PA in healthy controls, MCT rats with placebo, and MCT rats with

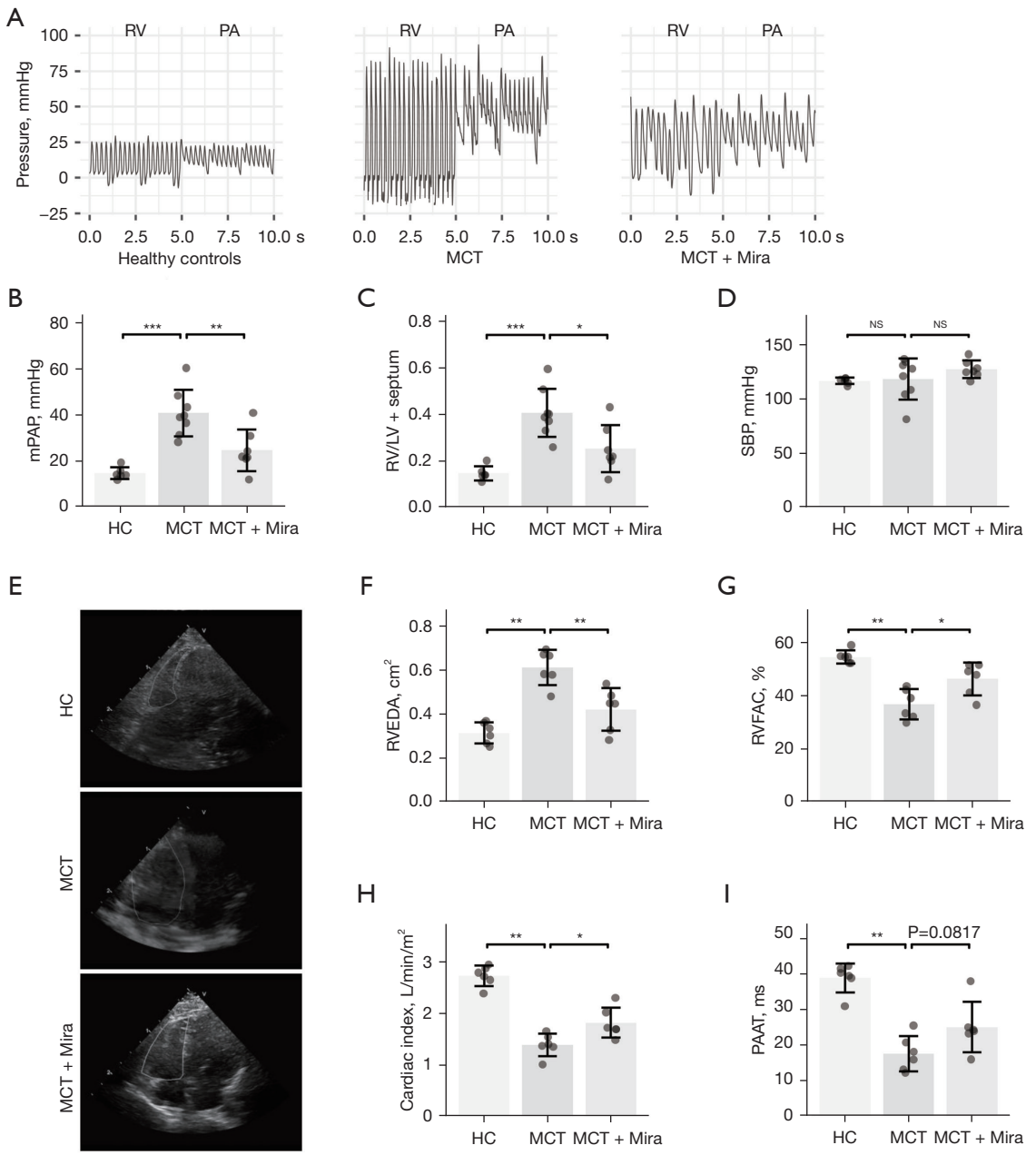

Figure 2 Mirabegron reduces RV pressure and prevents RV deterioration. (A) Representative pressure curves of RV and PA in groups of healthy controls, MCT rats, and MCT rats with mirabegron treatment. (B) Quantification of mPAP in the three groups. (C) Quantification of Fulton index (RV/LV + septum) in the three groups. (D) Quantification of systemic SBP in the three groups. (E) Representative four-chamber views of echocardiography in groups of healthy controls, MCT rats, and MCT rats with mirabegron treatment. (F) Quantitative analysis of RVEDA. (G) Quantitative analysis of RVFAC. (H) Quantitative analysis of cardiac index. (I) Quantitative analysis of PAAT. HC: healthy control; MCT: MCT rats; MCT + Mira: MCT rats with mirabegron treatment. Sample size: N=6–8 for each group in RHC analysis, N=6 for each group in data of echocardiography. *, P<0.05; **, P<0.01; ***, P<0.001. NS, non-significance; RV, right ventricular; LV, left ventricular; PA, pulmonary artery; MCT, monocrotaline; mPAP, mean pulmonary arterial pressure; SBP, systolic blood pressure; RVEDA, RV end-diastolic area; RVFAC, RV fractional area change; PAAT, pulmonary artery acceleration time; RHC, right heart catheterization.

mirabegron treatment (groups indicated in the figures). A remarkable reduction of pressure in the RV and PA was observed in MCT rats treated with mirabegron (MCT + Mira). According to the quantification of pressure data, mirabegron significantly reduced the mPAP in MCT rats (*Figure 2B*). Mirabegron effectively reduced RV hypertrophy [RV over left ventricular (LV) plus septum] in the MCT rats (*Figure 2C*). Systemic SBP showed no difference among the three groups (*Figure 2D*). No change in SBP was observed in mirabegron-treated rats of either healthy or MCT rats (Figure S1). The RV structural and functional changes of the rats were evaluated by echocardiography. The representative four-chamber views of echocardiography are presented in *Figure 2E*. The white delineations in *Figure 2E* indicate the RV area. There were increased RVEDA (*Figure 2F*), as well as decreased RVFAC (*Figure 2G*), CI (*Figure 2H*), and PAAT (*Figure 2I*) in MCT rats. These parameters were reflective of RV dilation and systolic function, cardiac function, and PA pressure. The B3AR agonist mirabegron reduced RV dilation (RVEDA), increased RV and cardiac function (RVFAC and CI), and reduced PA pressure (PAAT) (*Figure 2F-2I*).

Mirabegron reduced fibrosis and hypertrophy in the overloaded RV

Fibrosis and hypertrophy of the RV myocardium were assessed using SR staining and WGA fluorescent staining, respectively. Representative images are shown in *Figure 3A*. The levels of collagen 1, tissue inhibitor of metalloproteinases 1 (TIMP1), and brain natriuretic peptide (BNP) in the RV were assessed by immunoblotting (*Figure 3B*). Notably, fibrotic and hypertrophic development was observed in the RV myocardium of MCT rats. The pathological degeneration was prevented by mirabegron treatment. *Figure 3C* and *Figure 3D* present the quantification of SR staining and WGA fluorescent staining. The increased SR percentage and cardiomyocyte diameter in MCT rats were significantly reduced by mirabegron. Increased collagen 1 (*Figure 3E*), TIMP1 (*Figure 3F*), and BNP (*Figure 3G*) were observed in the RV of MCT rats, and were reduced by mirabegron treatment (*Figure 3E-3G*). The pathetical and molecular changes supported the protective role of mirabegron in the RV in MCT rats.

Mirabegron suppressed Drp1 and promoted AMPK in the overloaded RV

To figure out the potential molecular regulation of mirabegron on the AMPK/Drp1 signaling in the overloaded RV, the phosphorylation of the key molecules was examined. Representative immunoblots of AMPK, Drp1, mTOR, and their phosphonates are shown in *Figure 4A*. Quantification bar charts of the intensity of the immunoblots are presented in *Figure 4B-4E*. Mirabegron reduced the elevated phosphorylation of Drp1 at Ser616 (p-Drp1^{Ser616} in *Figure 4B*), and increased the phosphorylation of Drp1 at Ser637 (p-Drp1^{Ser637}), in MCT rats (*Figure 4C*). The total Drp1 expression was not changed among the groups (*Figure 4D*). Mirabegron also enhanced AMPK phosphorylation (p-AMPK), and reduced the phosphorylation of its downstream target mTOR (p-mTOR), in the RV of MCT rats (*Figure 4E*). The data showed that mirabegron activated AMPK and suppressed Drp1, suggesting its regulatory role in metabolic modulation and mitochondrial dynamics.

Mirabegron regulated AMPK and Drp1 in hypertrophied cardiomyocytes

Ang II induced hypertrophy model in H9c2 cells was used to further confirm the regulatory role of mirabegron on AMPK and Drp1. The phosphorylation of AMPK (and its downstream target mTOR) and Drp1 (at Ser 616 and Ser 637) were assessed and the representative immunoblots were presented in *Figure 5A*. Mirabegron (10 μM) decreased p-Drp1^{Ser616} (*Figure 5B*), and increased p-Drp1^{Ser637} (*Figure 5C*) in Ang II-treated H9c2 cells. AMPK inhibitor Compound C (Dorsomorphin, 10 μM) reversed the mirabegron-induced changes of Drp1 phosphorylation in Ang II-treated H9c2 cells. The level of total Drp1 was not altered by Ang II, mirabegron, and Compound C in H9c2 cells (*Figure 5D*). Mitochondrial division inhibitor Mdivi-1 was used as a reference for Drp1 regulation. Mdivi-1 (20 μM) decreased p-Drp1^{Ser616} and reduced the total Drp1 level in Ang II-treated H9c2 cells. In terms of AMPK signaling, Mirabegron (10 μM) increased p-AMPK and reduced p-mTOR in Ang II-treated H9c2 cells (*Figure 5E,5F*). Compound C (10 μM) reduced the mirabegron-induced activation of AMPK signaling. The results suggested that mirabegron regulates Drp1 phosphorylation through AMPK activation. The potential mechanisms of the effect of mirabegron on the failing RV are depicted in a sketch (*Figure 6*).

Discussion

The current study demonstrated that mirabegron

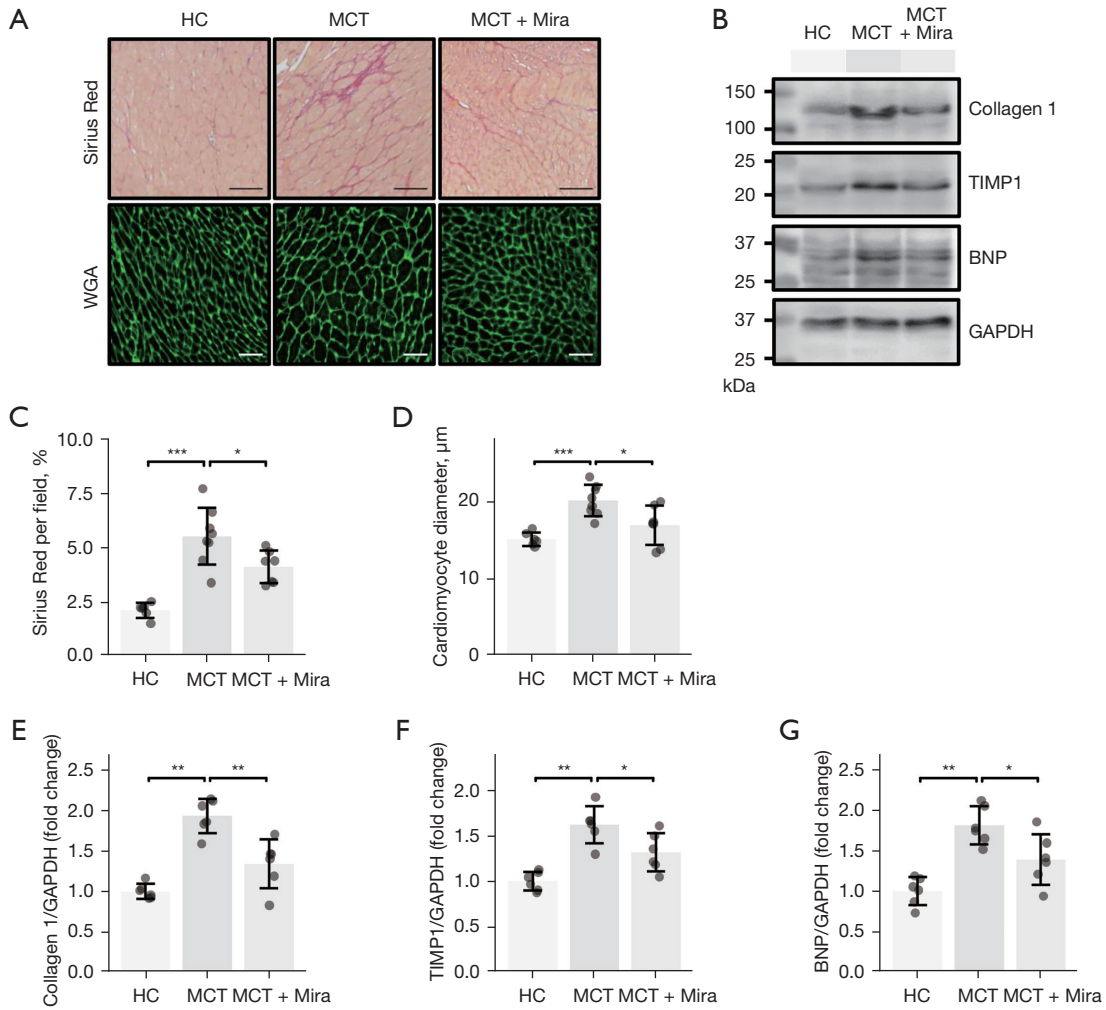

Figure 3 Mirabegron attenuated RV hypertrophy and fibrosis, and reduced RV structural and functional deterioration. (A) Representative Sirius Red (upper row) and WGA staining (lower row) images of the RV free wall in groups of healthy controls, MCT rats, and MCT rats with mirabegron treatment. Scale bar = 100 μm in Sirius Red images; Scale bar =50 μm in WGA images. (B) Representative immunoblots of Collagen 1, TIMP1, and BNP in the RV in groups of healthy controls, MCT rats, and MCT rats with mirabegron treatment. (C) Quantification of Sirius Red percentage of RV free wall in the three groups. (D) Analysis of cardiomyocyte diameter from WGA staining in RV free wall in the three groups. (E) Quantitative analysis of immunoblots of Collagen 1. (F) Quantitative analysis of immunoblots of TIMP1. (G) Quantitative analysis of immunoblots of BNP. HC: healthy control; MCT: MCT rats; MCT + Mira: MCT rats with mirabegron treatment. Sample size: N=8 for each group in histology data. N=6 for each group in immunoblotting data. *, P<0.05; **, P<0.01; ***, P<0.001. WGA, wheat germ agglutinin; TIMP1, tissue inhibitor of metalloproteinases 1; MCT, monocrotaline; BNP, brain natriuretic peptide; RV, right ventricular.

reduces PA pressure, and diminishes RV fibrosis and RV cardiomyocyte hypertrophy in MCT rats. Notably, mirabegron reboots AMPK and reduces Drp1 activation in RV cardiomyocytes, suggesting its role in promoting metabolic efficiency in the myocardium of the failing RV.

Although targeting pulmonary vascular remodeling has been the dominant strategy for PH therapeutics, prevention of RV dysfunction has emerged as a promising treatment option (3). RV-oriented studies are driven by strong clinical evidence demonstrating that RV function is highly correlated with survival and prognosis in patients with PH (21). Therefore, increasing efforts have been made

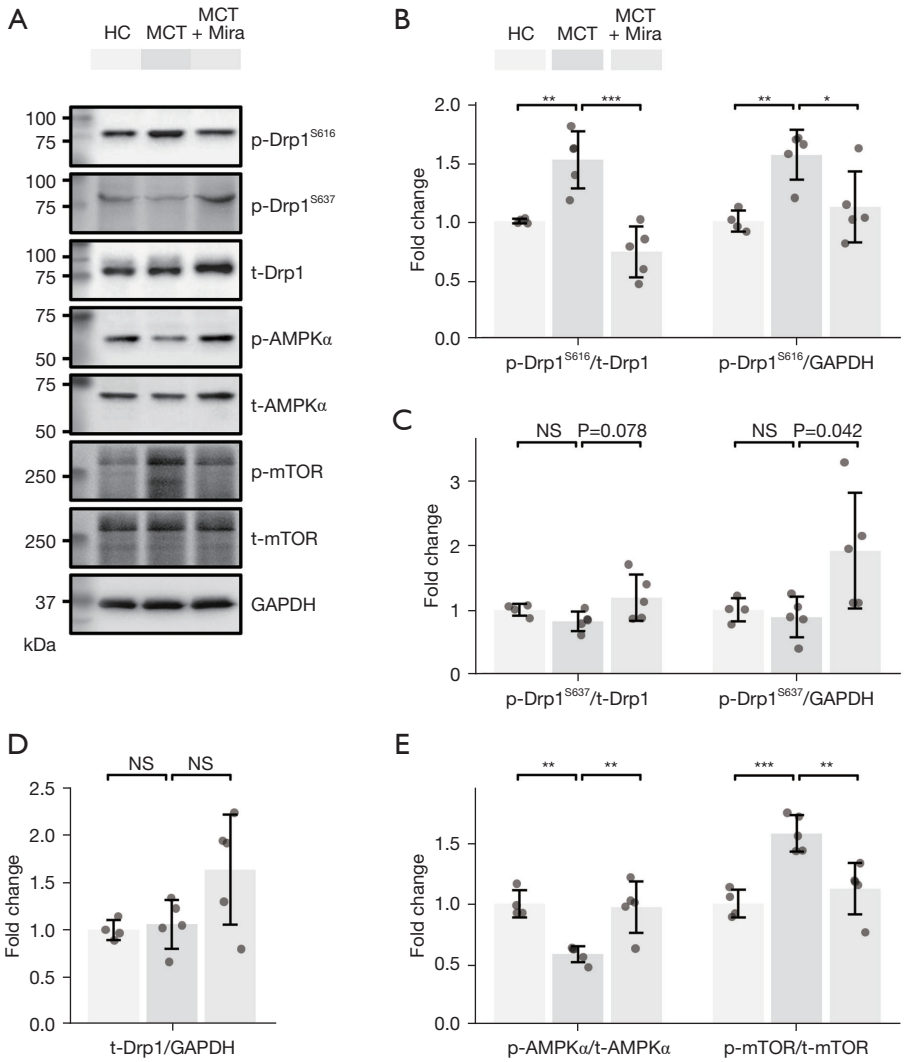

Figure 4 Mirabegron suppresses Drp1 and enhances AMPK signaling in the overload RV. (A) Representative immunoblots of Drp1, AMPK, mTOR, and their phosphorylated forms (p-Drp1 at Ser616 and Ser637, p-AMPK at Thr172, and p-mTOR at Ser2448) in the RV in groups of healthy controls, MCT rats, and MCT rats with Mirabegron treatment. (B) Quantification of the immunoblots of phospho-Drp1 at Ser616 (p-Drp1^{S616}). The phosphorylation is presented as the ratio of p-Drp1^{S616} to total Drp1 or GAPDH (p-Drp1^{S616}/t-Drp1 or p-Drp1^{S616}/GAPDH). (C) Quantification of the immunoblots of p-Drp1 at Ser^{637} (p-Drp1^{S637}). The phosphorylation is presented as the ratio of p-Drp1^{S637} to total Drp1 or GAPDH (p-Drp1^{S637}/t-Drp1 or p-Drp1^{S637}/GAPDH) (D) Quantification of the immunoblots of total Drp1. (E) Quantitative analysis of the phosphorylation of AMPK and mTOR. HC: healthy control; MCT: MCT rats; MCT + Mira: MCT rats with mirabegron treatment. Sample size: N=4–5 for each group. Significance codes: *, P<0.05; **, P<0.01; ***, P<0.001. NS, non-significance; Drp1, dynamin-related protein 1; AMPK, AMP-activated protein kinase; RV, right ventricular.

to decipher the molecular mechanisms underlying RV pathogenic changes, such as fibrosis and hypertrophy.

B3AR has been identified in the RV (22). Although the B3AR was proposed to be cardioprotective (23), there is limited and inconsistent knowledge referring the B3AR to the right side of the heart (11,12,22,24). Increased B3AR expression was observed in the pathological myocardium (25-27). In our study, increased B3AR expression was observed in the overloaded RV in MCT rats. The increase of B3AR expression was confirmed both in protein and

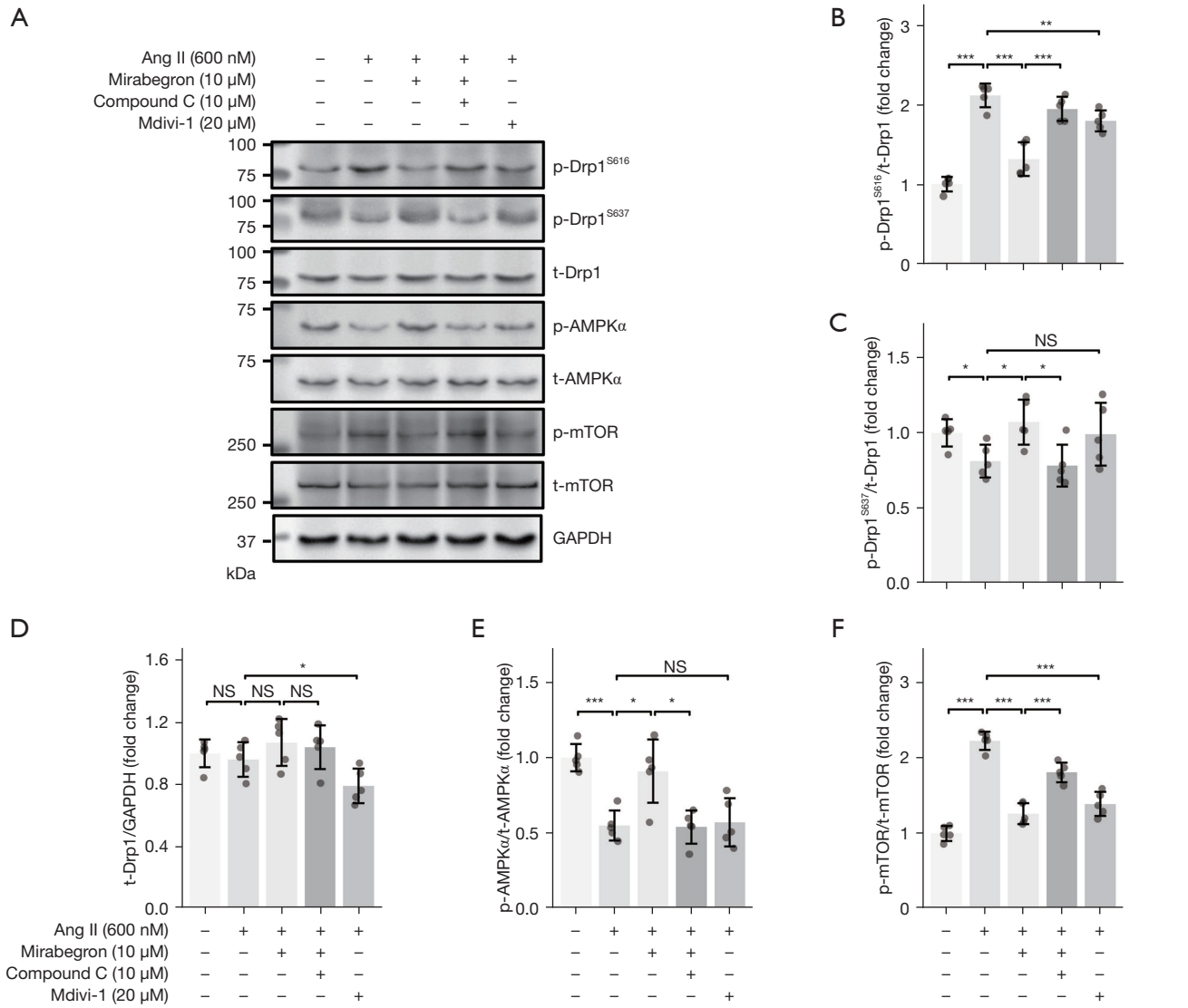

Figure 5 Mirabegron suppresses Drp1 and enhances the AMPK signaling in hypertrophied cardiomyocytes. H9c2 cardiomyocyte cells were treated with Ang II (600 mM), as well as mirabegron (10 μM), AMPK inhibitor Compound C (10 μM), and Drp1 inhibitor Mdivi-1 (20 μM), as indicated with "–" or "+" in the figure. Five groups were included in the cell experiments. (A) Representative immunoblots of Drp1, AMPK, mTOR, and their phosphorylated forms (p-Drp1 at Ser616 and Ser637, p-AMPKα at Thr172, and p-mTOR at Ser2448) in the groups. (B) Quantification of the p-Drp1 at Ser616 (presented as p-Drp1^{S616}/t-Drp1). (C) Quantification of the p-Drp1 at Ser637 (presented as p-Drp1^{S637}/t-Drp1). (D) Quantification of the immunoblots of total Drp1. (E) Quantitative analysis of the p-AMPKα. (F) Quantitative analysis of the p-mTOR. Sample size: N=5 for each group. Significance codes: *, P<0.05; **, P<0.01; ***, P<0.001. NS, non-significance; Drp1, dynamin-related protein 1; AMPK, AMP-activated protein kinase.

RNA levels. A study showed that B3AR agonists could further promote the increase of B3AR expression in the failing heart (28). Our data was in line with the results in this study. MCT rats with mirabegron treatment had a further increase in the expression of B3AR in the RV. The upregulation of B3ARs could serve as a compensatory mechanism to make up for the metabolic inefficiency in the pathological myocardium. More research is needed to confirm the link between B3ARs and cardiac metabolism regulation.

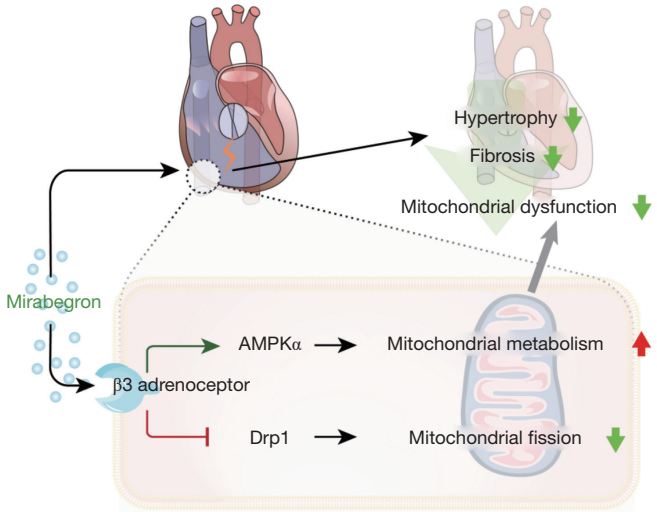

Figure 6 Proposed mechanism of the treatment effect of mirabegron on the RV. Mirabegron reduces RV pathological changes and restores RV metabolic status. The beneficial effect could be attributed to (I) promotion of mitochondrial metabolism through AMPK activation; and (II) suppression of mitochondrial fission by inhibiting Drp1. Drp1, dynamin-related protein 1; AMPK, AMP-activated protein kinase; RV, right ventricular.

In contrast to the physiological role of β1 and β2 adrenoceptors, B3AR has been shown to prevent adrenergic overactivation (29). Genetic manipulation of the B3AR in cardiomyocytes in mice demonstrated that upregulating cardiac B3AR reduced cardiac hypertrophy and fibrosis in the failing heart, through modulating oxidant stress-related paracrine signaling (10,30). Herein, we demonstrated that the B3AR agonist mirabegron attenuated the fibrotic and hypertrophic remodeling and restored the functional status of the overloaded RV in experimental PH. The findings are in line with a study that investigated mirabegron in a porcine PH model of pulmonary vein banding (12). Using this porcine model of PH, the researchers found that B3AR agonists reduced pulmonary vascular resistance, decreased RV systolic volume, and improved RV ejection fraction (12). Pathological changes and molecular mechanisms of the RV were not examined in the mentioned study. Our work confirmed mirabegron's treatment effect on the overloaded RV and provided preliminary insight into the underlying mechanism. There is an ongoing clinical trial aiming to evaluate the efficacy and safety of mirabegron in patients with PH secondary to heart failure (SPHERE-HF NCT02775539) (31). The results of this study have not been released yet. Our data may offer preclinical insight supporting the use of mirabegron in PH patients.

It should be noted that there might be off-target effects of mirabegron on adrenoceptor β1/β2 (11). Although mirabegron is a potent agonist of B3AR, it showed lower selectivity for B3AR compared to agonists such as Vibegron and CL316,243 (32,33). To diminish the off-target effect of mirabegron, we estimated the animal dose from a safe human dose (14) and also reviewed the literature to adopt an appropriate dose of mirabegron in rats (15,16). In addition, the potential impact of mirabegron on SBP was investigated and no change in SBP was observed in mirabegron-treated rats in our study. Some researchers reported that antagonism of the B3AR (SR59230A) could improve RV function in rats with MCT-induced PH by reducing nitric oxide synthase (22). The discrepancy should be interpreted with caution because the role of the B3AR in RV is not fully understood. The B3AR may play a pleiotropic role in cardiac pathology. The pharmacological nature of the antagonist used in the mentioned study was not well-defined as well. It should also be noted that the majority of studies have reported that B3AR agonism leads to the prevention of cardiac hypertrophy and failure by reducing superoxide and increasing nitric oxide production (10,34).

Beyond its role in redox homeostasis, the link between B3ARs and mitochondrial dysfunction has been studied. The activation of B3ARs reduces mitochondrial dysfunction in hypertrophic cardiomyocytes through activating AMPK signaling and inhibiting autophagy (24).

Our study offers a similar mechanism insight into the RV myocardium. We observed enhanced AMPK signaling in the overloaded RV of MCT rats treated with mirabegron, implying enhanced metabolism by mirabegron treatment in RV myocardium.

Disturbed mitochondrial dynamics have been identified as part of the dysfunctional RV metabolism (7). RV ischemia/reperfusion induces mitochondrial fission. Targeting mitochondrial fission using Drp1 inhibitors (Mdivi-1 and P110) attenuated the ischemia/reperfusion injury in the RV (35). More relevant to our study, increased mitochondrial fission has been linked to excessive RV fibrosis. Suppressing Drp1 avoids mitochondrial fission and decreases RV fibrosis (7). The activity of Drp1 is enhanced by phosphorylation at serine 616 (p-Drp1^{Ser616}), and is suppressed by phosphorylation at serine 637 (p-Drp1^{Ser637}) (36). Both phosphorylating sites were investigated in our study. Mirabegron treatment decreased p-Drp1^{Ser616} and enhanced p-Drp1^{Ser637} in the failing RV, or the hypertrophied cardiomyocytes, which together led to an inhibition of Drp1 activity. According to our findings, the molecular basis underlying the therapeutic effect could be attributed to Drp1 inhibition. A recent congress abstract claimed that mirabegron reduced endothelial mitochondrial fragmentation by restoring mitochondrial fission/fusion dynamics in PH models of MCT rats and hypoxic mice (37). Our data showed that mirabegron suppressed Drp1-induced mitochondrial fission in the RV myocardium in PH. These results, therefore, suggest that mirabegron could improve mitochondrial metabolism in both pulmonary vasculature and RV myocardium.

Overall, the upregulation of B3ARs in the overloaded RV could serve as an adaptive mechanism to improve metabolic efficiency. Activating B3ARs using mirabegron reduces RV hypertrophy and fibrosis, and improves RV hemodynamics. This therapeutic effect is associated with AMPK activation and Drp1 suppression. Taken together, current evidence supports mirabegron as a viable treatment option for RV dysfunction in patients with PH.

Conclusions

Mirabegron, a selective B3AR agonist, prevents RV hypertrophy and fibrotic remodeling in rats with MCT-induced PH. Mirabegron could enhance metabolic efficiency in dysfunctional RV myocardium by activating AMPK and suppressing Drp1. Mirabegron serves as a promising medication for improving the RV in PH.

Acknowledgments

We appreciate Dr. Tingting Wu for providing expertise and technical support in echocardiography.

Funding: This study was supported by the Natural Science Foundation Project of Hunan province, China (grant No. 2020JJ4634), and the National Natural Science Foundation of China (grant No. 82000058).

Footnote

Reporting Checklist: The authors have completed the ARRIVE reporting checklist. Available at https://cdt.amegroups.com/article/view/10.21037/cdt-22-274/rc

Data Sharing Statement: Available at https://cdt.amegroups.com/article/view/10.21037/cdt-22-274/dss

Conflicts of Interest: All authors have completed the ICMJE uniform disclosure form (available at https://cdt.amegroups.com/article/view/10.21037/cdt-22-274/coif). The authors have no conflicts of interest to declare.

Ethical Statement: The authors are accountable for all aspects of the work in ensuring that questions related to the accuracy or integrity of any part of the work are appropriately investigated and resolved. Experiments were performed under a project license (No. CSU-2022-01-0122) granted by the Animal Ethics Committee of Central South University, in accordance with the Animals (Scientific Procedures) Act 1986 for the care and use of animals.

References

1. Vonk Noordegraaf A, Chin KM, Haddad F, et al. Pathophysiology of the right ventricle and of the pulmonary circulation in pulmonary hypertension: an update. Eur Respir J 2019;53:1801900.

2. Westerhof BE, Saouti N, van der Laarse WJ, et al. Treatment strategies for the right heart in pulmonary hypertension. Cardiovasc Res 2017;113:1465-73.
3. Konstam MA, Kiernan MS, Bernstein D, et al. Evaluation and Management of Right-Sided Heart Failure: A Scientific Statement From the American Heart Association. Circulation 2018;137:e578-622.
4. Jin JY, Wei XX, Zhi XL, et al. Drp1-dependent mitochondrial fission in cardiovascular disease. Acta Pharmacol Sin 2021;42:655-64.
5. Chen KH, Dasgupta A, Lin J, et al. Epigenetic Dysregulation of the Dynamin-Related Protein 1 Binding Partners MiD49 and MiD51 Increases Mitotic Mitochondrial Fission and Promotes Pulmonary Arterial Hypertension: Mechanistic and Therapeutic Implications. Circulation 2018;138:287-304.
6. Li J, Wang Y, Wang Y, et al. Pharmacological activation of AMPK prevents Drp1-mediated mitochondrial fission and alleviates endoplasmic reticulum stress-associated endothelial dysfunction. J Mol Cell Cardiol 2015;86:62-74.
7. Tian L, Potus F, Wu D, et al. Increased Drp1-Mediated Mitochondrial Fission Promotes Proliferation and Collagen Production by Right Ventricular Fibroblasts in Experimental Pulmonary Arterial Hypertension. Front Physiol 2018;9:828.
8. Roy R, Koch WJ. Not All β-Receptors Appear the Same in Heart Failure: Emergence of β3-Agonists as a Therapeutic Option. Circ Heart Fail 2022;15:e009685.
9. Yang W, Wei X, Su X, et al. Depletion of β3-adrenergic receptor induces left ventricular diastolic dysfunction via potential regulation of energy metabolism and cardiac contraction. Gene 2019;697:1-10.
10. Belge C, Hammond J, Dubois-Deruy E, et al. Enhanced expression of β3-adrenoceptors in cardiac myocytes attenuates neurohormone-induced hypertrophic remodeling through nitric oxide synthase. Circulation 2014;129:451-62.
11. Dehvari N, da Silva Junior ED, Bengtsson T, et al. Mirabegron: potential off target effects and uses beyond the bladder. Br J Pharmacol 2018;175:4072-82.
12. García-Álvarez A, Pereda D, García-Lunar I, et al. Beta-3 adrenergic agonists reduce pulmonary vascular resistance and improve right ventricular performance in a porcine model of chronic pulmonary hypertension. Basic Res Cardiol 2016;111:49.
13. Rosa GM, Ferrero S, Nitti VW, et al. Cardiovascular Safety of β3-adrenoceptor Agonists for the Treatment of Patients with Overactive Bladder Syndrome. Eur Urol 2016;69:311-23.
14. Nair AB, Jacob S. A simple practice guide for dose conversion between animals and human. J Basic Clin Pharm 2016;7:27-31.
15. Noh TI, Shim JS, Kang SG, et al. Effects of β3-adrenoceptor agonist on acute urinary retention in a rat model. World J Urol 2021;39:4427-33.
16. Kovács ZZA, Szűcs G, Freiwan M, et al. Comparison of the antiremodeling effects of losartan and mirabegron in a rat model of uremic cardiomyopathy. Sci Rep 2021;11:17495.
17. Siti HN, Jalil J, Asmadi AY, et al. Rutin Modulates MAPK Pathway Differently from Quercetin in Angiotensin II-Induced H9c2 Cardiomyocyte Hypertrophy. Int J Mol Sci 2021;22:5063.
18. Huang R, Liu Y, Ciotkowska A, et al. Concentration-dependent alpha1-Adrenoceptor Antagonism and Inhibition of Neurogenic Smooth Muscle Contraction by Mirabegron in the Human Prostate. Front Pharmacol 2021;12:666047.
19. Vucicevic L, Misirkic M, Janjetovic K, et al. Compound C induces protective autophagy in cancer cells through AMPK inhibition-independent blockade of Akt/mTOR pathway. Autophagy 2011;7:40-50.
20. Dai W, Wang G, Chwa J, et al. Mitochondrial division inhibitor (mdivi-1) decreases oxidative metabolism in cancer. Br J Cancer 2020;122:1288-97.
21. Naeije R, Ghio S. More on the right ventricle in pulmonary hypertension. Eur Respir J 2015;45:33-5.
22. Sun J, Cheng J, Ding X, et al. β3 adrenergic receptor antagonist SR59230A exerts beneficial effects on right ventricular performance in monocrotaline-induced pulmonary arterial hypertension. Exp Ther Med 2020;19:489-98.
23. Cannavo A, Koch WJ. Targeting β3-Adrenergic Receptors in the Heart: Selective Agonism and β-Blockade. J Cardiovasc Pharmacol 2017;69:71-8.
24. Dubois-Deruy E, Gelinas R, Beauloye C, et al. Beta 3 adrenoreceptors protect from hypertrophic remodelling through AMP-activated protein kinase and autophagy. ESC Heart Fail 2020;7:920-32.
25. Michel LYM, Farah C, Balligand JL. The Beta3 Adrenergic Receptor in Healthy and Pathological Cardiovascular Tissues. Cells 2020;9:2584.
26. Zhao Q, Wu TG, Jiang ZF, et al. Effect of beta-blockers on beta3-adrenoceptor expression in chronic heart failure. Cardiovasc Drugs Ther 2007;21:85-90.
27. Zhao Q, Zeng F, Liu JB, et al. Upregulation of β3-

adrenergic receptor expression in the atrium of rats with chronic heart failure. J Cardiovasc Pharmacol Ther 2013;18:133-7.
28. Miao G, Chen Z, Fang X, et al. Relationship between the autoantibody and expression of β3-adrenoceptor in lung and heart. PLoS One 2013;8:e68747.
29. Michel LYM, Balligand JL. New and Emerging Therapies and Targets: Beta-3 Agonists. Handb Exp Pharmacol 2017;243:205-23.
30. Hermida N, Michel L, Esfahani H, et al. Cardiac myocyte β3-adrenergic receptors prevent myocardial fibrosis by modulating oxidant stress-dependent paracrine signaling. Eur Heart J 2018;39:888-98.
31. Garcia-Lunar I, Blanco I, Fernández-Friera L, et al. Design of the β3-Adrenergic Agonist Treatment in Chronic Pulmonary Hypertension Secondary to Heart Failure Trial. JACC Basic Transl Sci 2020;5:317-27.
32. Brucker BM, King J, Mudd PN Jr, et al. Selectivity and Maximum Response of Vibegron and Mirabegron for β3-Adrenergic Receptors. Curr Ther Res Clin Exp 2022;96:100674.
33. Beauval JB, Guilloteau V, Cappellini M, et al. Comparison of the effects of β3 -adrenoceptor agonism on urinary bladder function in conscious, anesthetized, and spinal cord injured rats. Neurourol Urodyn 2015;34:578-85.
34. Niu X, Watts VL, Cingolani OH, et al. Cardioprotective effect of beta-3 adrenergic receptor agonism: role of neuronal nitric oxide synthase. J Am Coll Cardiol 2012;59:1979-87.
35. Tian L, Neuber-Hess M, Mewburn J, et al. Ischemia-induced Drp1 and Fis1-mediated mitochondrial fission and right ventricular dysfunction in pulmonary hypertension. J Mol Med (Berl) 2017;95:381-93.
36. Sharp WW, Fang YH, Han M, et al. Dynamin-related protein 1 (Drp1)-mediated diastolic dysfunction in myocardial ischemia-reperfusion injury: therapeutic benefits of Drp1 inhibition to reduce mitochondrial fission. FASEB J 2014;28:316-26.
37. Oliver E, Rocha SF, Spaczynska M, et al. Beta3-adrenergic stimulation restores endothelial mitochondrial dynamics and prevents pulmonary arterial hypertension. Eur Heart J 2020;41:ehaa946.3808.

Cite this article as: Zhao L, Luo H, Li T, Zhao X, Liu Y. β3 adrenoceptor agonist mirabegron protects against right ventricular remodeling and drives Drp1 inhibition. Cardiovasc Diagn Ther 2022;12(6):815-827. doi: 10.21037/cdt-22-274

